Experiments in Fluids 16, 248–254 (1994)

Experiments in Fluids

The structure of compressible starting vortices

S. Lee* and **D. Bershader†**

Department of Aeronautics and Astronautics, Stanford University, Stanford, California 94305

Received: 19 October 1992 / Accepted: 8 June 1993

Abstract. The structures of highly two-dimensional shock-induced compressible starting vortices were investigated. Density distributions across the vortex were measured by dual-pulsed holographic interferometry. Pressure profiles of the vortex were measured by fast-response miniature Kulite transducers. From these two independent measurements the velocity profile was calculated using the radial momentum equation. The detailed vortex structure is similar to that from the tip of a wing and consists of four well-defined regions: a core region, a logarithmic region, a transition region, and an inviscid region. The distribution of circulation of the vortices can be expressed by a set of empirical formulae. The proportionality constants of the logarithmic region were found to be 0.43 ± 0.01 for three different two-dimensional vortices.

1 Introduction

The structure of convecting vortices, such as trailing vortices from a wing tip or leading-edge vortices, has been an important topic of aerodynamic research. Vortices trailing from a rotating blade or generated by the leading edge of an aircraft are inherently three-dimensional and not persistent along a straight vortex axis. Hoffman and Joubert (1963) investigated the trailing vortex by assuming it to be completely independent of viscosity effects and found conditions when a universal distribution of circulation can be determined in the inner region of the vortex. Nielsen and Schwind (1971) extended Hoffman and Joubert's experiment. They divided the vortices behind the aircraft into three stages; (1) the rolling-up stage, (2) the equilibrium stage, and (3) the interaction (or decay) stage. A theory for the equilibrium stage was developed through experimental correlations of the radial circulation distribution. Based on the idea of Hoffman and Joubert, they also divided the equilibrium vortex into four distinct regions, analogous to the turbulent boundary layer:

1. A core or inner region, analogous to the viscous sublayer in the turbulent boundary layer. This region rotates like a solid body and the circulation is proportional to the square of the distance from the center;
2. A logarithmic region, analogous to the law of the wall in the turbulent boundary layer. The tangential velocity reaches a maximum in this region and the circulation is proportional to the logarithm of the distance from the center;
3. A transition region to the outer inviscid region, analogous to the defect law in the turbulent boundary layer. The circulation has been expressed in similar ways (Table 1), but the measured data generally do not fit any of these curves;
4. The irrotational region in which the circulation is constant.

Figure 1 is a schematic sketch of a typical trailing-vortex layer, which shows the four distinct regions mentioned above. Several researchers have investigated the vortex structure at the equilibrium stage with the assumption that the vortex is locally indistinguishable from a two-dimensional line vortex; i.e., the curvature of the vortex is ignored and the measured vortex is axisymmetric about its axis. The results are summarized in Table 1 by expressing the ratio of circulation to the maximum circulation (a value at the inviscid region), Γ/Γ_{max}, as a function of the ratio of distance from the vortex center to the core radius, r/a_0. But these formulae involve a variety of coefficients representing an equilibrium solution, which may be considered as a limiting case from the viewpoint of vortex persistency. In the present study, we produced a highly two-dimensional vortex in a shock tube and measured the structure of the vortex to determine the coefficients of the formula.

* Presently at U.S. Army Aeroflightdynamics Directorate, ATCOM, NASA-Ames Research Center, Moffett Field, CA 94035
† Professor

Table 1. Literature reports of vortex structure at equilibrium stage

	Core region (Γ/Γ_{max})	Logarithmic region (Γ/Γ_{max})	Defect region (Γ/Γ_{max})
Hoffman & Joubert (1963)	$1.0\,(r/a_0)^2$	$.51\ln(r/a_0)+.55$	—
Nielsen & Schwind (1971)	$.78\,(r/a_0)^2$	$.49\ln(r/a_0)+.53$	$1-2.4\,e^{-1.4(r/a_0)}$
Corsiglia et. al. (1973)	$.88\,(r/a_0)^2$	$.44\ln(r/a_0)+.44$	$1-.85\,e^{-.59(r/a_0)}$
Uberoi (1979)	—	$.53\ln(r/a_0)+.35$	—
Phillips (1981)	$1.77\,(r/a_0)^2-1.05\times(r/a_0)^4+.27\,(r/a_0)^6$	$.50\ln(r/a_0)+.50$	—
Tung et. al. (1983)	$.80\,(r/a_0)^2$	$.39\ln(r/a_0)+.32$	$1-.80\,e^{-.65(r/a_0)}$

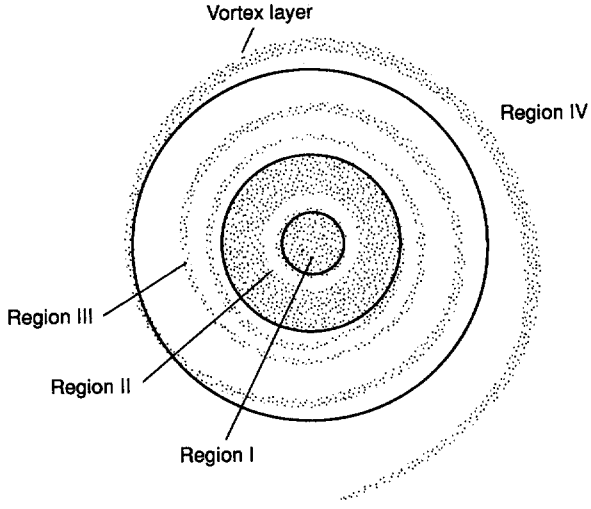

Fig. 1. Schematic sketch of the structure of a trailing vortex layer [Tung, et al.]

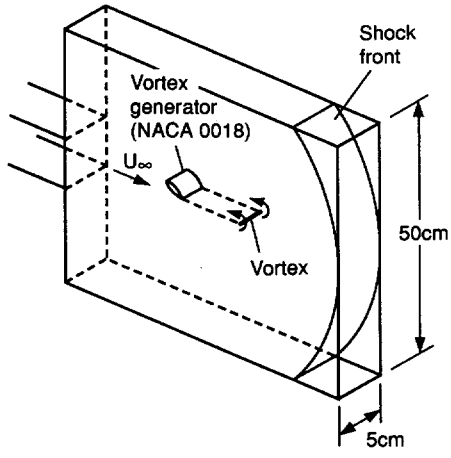

Fig. 2. Schematic of the test section and the generation of a single starting vortex

2 Experimental methods

2.1 Vortex generation and measurement

How to produce a single vortex (or vortex line) and how to measure the vortex structure are very critical problems in this study. A fixed angle-of-attack airfoil in the shock tube was taken as a vortex generator to make a shock-generated starting vortex. This method provides a very axisymmetrical and clean single vortex, which can be taken to be almost two-dimensional.

A shock tube, having a rectangular test section, was designed to investigate the structure of compressible starting vortices. Shown schematically in Fig. 2 is the test section with a vortex generator, the shock, and the generated vortex. The driven section of the shock tube has a square (5 × 5 cm) cross section. The test section, open to the atmosphere, is located at the end of the driven section. The planar geometry allows the shock to diffract only in a cylindrical fashion, as illustrated in Fig. 2; thus, the 2D feature of the flow-field is retained. Plexiglass windows measuring 25 cm × 36 cm are mounted parallel to each other and on opposite sides of the test section. For the vortex generator, a NACA 0018 airfoil was used, 3.8 cm long and 5 cm wide. The duration time of a quasi-uniform flow after a shock passes is about 4 ms. To measure the

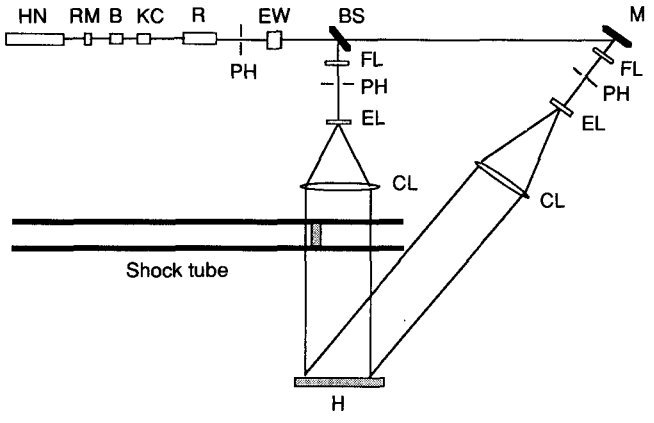

Fig. 3. Dual-pulsed holographic interferometry setup for density field measurement. HN: He-Ne laser, RM: 100% refractive mirror at 6943 Å, B: Brewster stack, KC: KDP crystal, R: Ruby rod, PH: Pin hole, EW: Etalon output window, BS: Beam splitter, M: Mirror, FL: Focusing lens, EL: Expanding lens, CL: Collimating lens, H: Holographic plate)

speed of the shock, two Kulite transducers (0.08 cm in diameter) were employed 65 cm upstream from the test section. For synchronizing the laser light source discharge with the shock motion, the signal from the second pressure transducer was used in conjuction with a digital delay generator, taking into account the inherent delay in the Q-switch laser pulse mechanism. The diaphragm pressure ratio was controlled from shot to shot by $\pm$ 1% by using polyester (mylar) sheets. To generate high-speed induced flow, without increasing the pressure in the high pressure section of the shock tube too much, helium was also used as a driver gas.

To measure the local velocity field of the vortex, either hot-wire or laser doppler velocimetry (LDV) could have been used. But, in the case of hot-wire measurements, the probe disturbs the flow field; hence we may expect some degree of error. On the other hand, LDV can measure the vortex flow field nonintrusively. This technique needs seed particles which are assumed to follow the nearly circular flow motion exactly. Unfortunately, these particles experience centripetal forces inside the vortex which cause their path to deviate from the flow. This is especially so inside the core region, the result being that we can hardly see sufficient particles to scatter the incoming light. Thus, this method looks inappropriate for the present investigation.

A less direct, but very reliable method was proposed by Mandella and Bershader (1987). This method involved the use of independent measurements of density and pressure distributions through the vortex to calculate the tangential velocity distribution by using the radial momentum equation. A dual-pulsed holographic interferometry technique [Fig. 3] was used for the density distribution and miniature pressure transducers (flush-mounted at the wall of the test section) were used to measure the pressure distribution across the vortex.

2.2 *DPHI (Dual-Pulsed Holographic Interferometry)*

In this application, the flow field is changing rapidly and so the exposure must be very short, compared with the characteristic time scale of the flow, to avoid a time averaging or blurring effect. Therefore, the light source should have good coherence properties and a short pulse duration. For this reason, a pulsed-ruby laser was selected as the light source for recording the hologram. When Q-switched, the laser produces a sufficiently coherent light pulse with an energy of 100 mJ and a duration of 10 ns. The laser beam is 2 mm in diameter at 6943Å and its properties are well-matched with the photographic materials available for holography. The coherence length Δl of the laser was found to be about 10 cm by changing the optical path length of the reference beam and monitoring the quality of the resultant holograms.

In dual-pulsed holographic interferometry interference takes place between the wave fronts reconstructed by the two holograms of the test section. The two holograms are recorded on the same photographic plate in two stages. The first one is made of the fluid at rest and the second one is made at the time of interest during the test. The resultant interferogram allows the flow to be visualized and analyzed. During both exposures, the only changing condition of the optical system is the density variation caused by the motion of the fluid flow inside the test section. Thus, only the object beam is different in each case. As a result, two holograms (i.e. two different diffraction patterns) are recorded on the same holographic plate by exposing both the object and the reference beams simultaneously [for details, see Lee (1992)].

The fringe shift is also related to the optical path by the relation

$$S(x, y) = N(x, y) - N_0(x, y)$$

$$= \frac{1}{\lambda_0} \int_0^L \{n(x, y, z) - n_0\} dz \tag{1}$$

where N is the fringe number, n is the refractive index, λ_0 is the vacuum wavelength of the monochromatic light source, and L is the span of the test section. The subscript 0 denotes the quantity at no flow. This relation has to be combined with the Gladstone-Dale relation

$$n(x, y, z) - 1 = K \rho(x, y, z) \tag{2}$$

where K is the Gladstone-Dale constant which is a property of the gas. Away from resonant wavelengths, this constant is a weak function of wavelength and is nearly independent of temperature and pressure under moderate

Table 2. Experimental conditions and freestream data

	Case I	Case II	Case III	Error estimation	Units
Shock speed	470	540	470	±15	m/sec
Angle of vortex generator	30	30	15	—	deg
Convection velocity of a vortex	180	260	180	±8	m/sec
Ambient density	1.78	2.20	1.78	±.05	kg/m^3
Ambient pressure	1.58×10^5	2.35×10^5	1.58×10^5	$\pm 5 \times 10^3$	N/m^2
Driven gas/ driver gas	Air/air	Air/he	Air/air	—	—

physical conditions. The fringe shift becomes

$$S(x, y)=\frac{K}{\lambda_0}\int_0^L \rho(x, y, z)dz-\frac{\rho_0 KL}{\lambda_0} \tag{3}$$

If we assume that the properties of the flow remain constant in the z direction,

$$S(x, y)=\frac{KL}{\lambda_0}\{\rho(x, y)-\rho_0\} \tag{4}$$

Clearly, the above equation shows the relation of the fringe shift distribution with the change in the density field of the flow.

For the present experiment, the change in density per unit fringe shift is

$$\frac{\Delta\rho}{S}=\frac{\lambda_0}{KL}=\frac{6943\times 10^{-10}\text{m}}{(2.3\times 10^{-4}\text{m}^3/\text{Kg})\times(5\times 10^{-2}\text{m})}$$
$$=0.0604\ \text{Kg/m}^3 \tag{5}$$

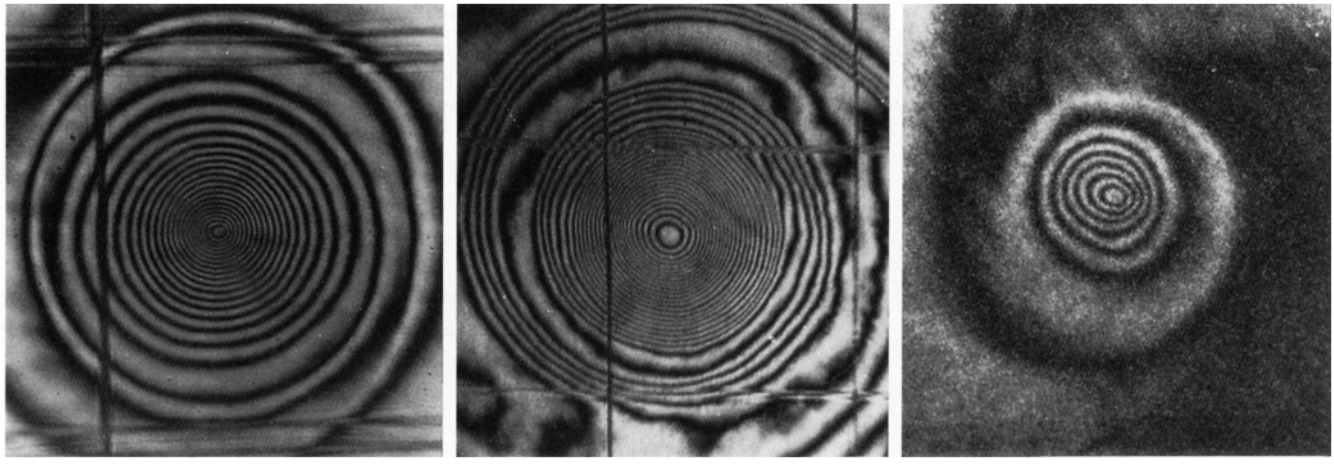

Fig. 4. Holographic Interferograms of three vortices, showing density contour lines

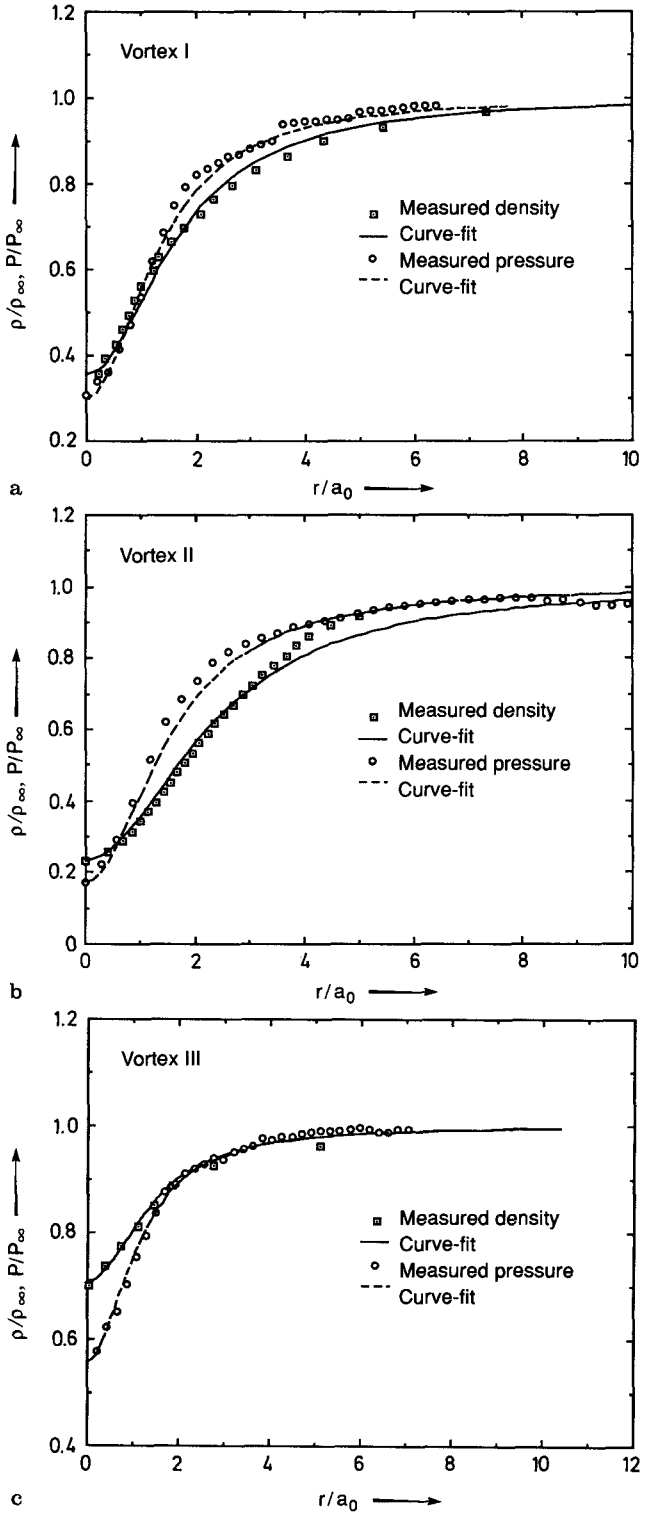

Fig. 5. Density and pressure measurements across each vortex

This means that the increment between fringes representing contours of constant density corresponds to about 1/20 of the atmospheric density. Silver halide emulsion plates were used for recording the holograms. A precise knowledge of the characteristics of photographic emulsion is needed in order to record holograms of good quality. Obviously the emulsion must be capable of resolving fringes at the carrier frequency of the hologram. In one case of the experiment, the offset angle is 23°. Since the wavelength of the ruby laser $\lambda = 694.3$ nm, the carrier frequency is therefore

$$f_y = \frac{\sin\theta}{\lambda} = \frac{\sin 23^\circ}{694.3 \times 10^{-6}}$$

$$= 562.8 \text{ lines/mm} \qquad (6)$$

This value is the minimal resolution requirement. Emulsion plates used in this experiment are the 10E75, made by Agfa-Gavaert, which have a resolution of 2800 lines/mm and are sensitive to the wavelength of the ruby laser. A sodium lamp was used for a light source for reconstruction of image plane holograms.

3 Results

3.1 Experimental conditions

The experimental investigation in this study was carried out using three different vortices, made by changing the angle of the vortex generator and the flow speed in the test section. As shown in Table 2, Vortex I was produced with the angle of attack of the vortex generator at 30° and the induced velocity in the test section at approximately 180 m/s (Mach number of the shock was 1.37 ± 0.05). This vortex is considered as the fundamental one in this study. Vortex II was produced by changing the induced velocity from 180 m/s to 260 m/s, with other conditions remaining the same. Vortex III was produced by changing the angle of the vortex generator from 30° to 15°, with other conditions remaining the same. Reducing the angle of attack of the vortex generator by half resulted in decreasing the circulation of the vortex approximately by half. The tangential velocity distribution of each vortex was measured indirectly by independent measurements of density and pressure distribution across the convecting vortex. The pressure signal was transformed into a spatial distribution by a Galilean transformation factor of 180 m/s (case I & III) or 260 m/s (case II). The modified Cauchy function was used to curve-fit the density and pressure data. The Reynolds numbers, based on the airfoil chord, of case I and II are estimated to be 0.9×10^6 and 1.3×10^6, respectively.

3.2 The vortex structures

Figure 4 shows holographic interferograms of three different single vortices, displaying density contour lines. In the interferograms, the fringe lines of the vortices are very

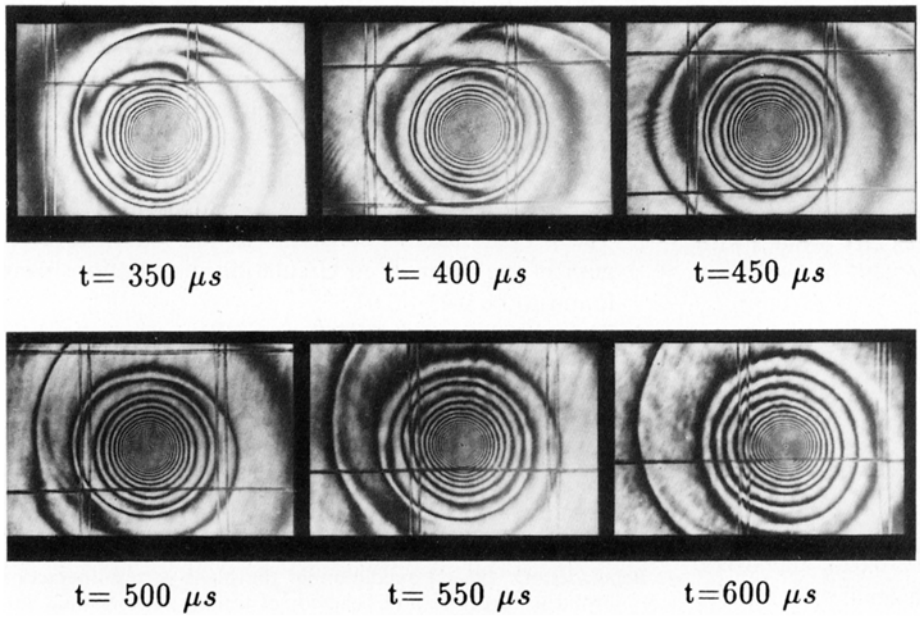

Fig. 6. The evolution of vortex I with time. (The interval between shots is 50 μs and corresponds to 10 core radii travel.)

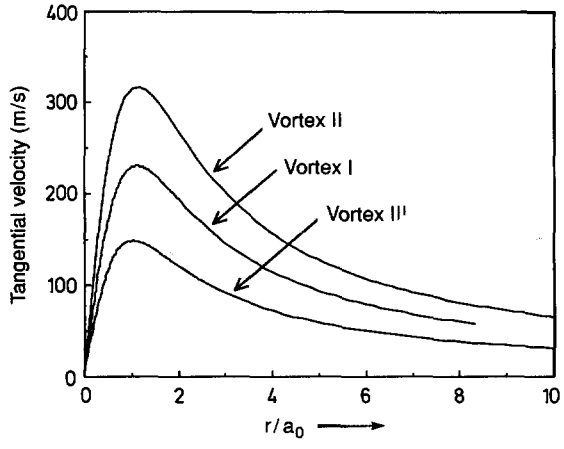

Fig. 7. Calculated tangential velocity profiles of three vortices

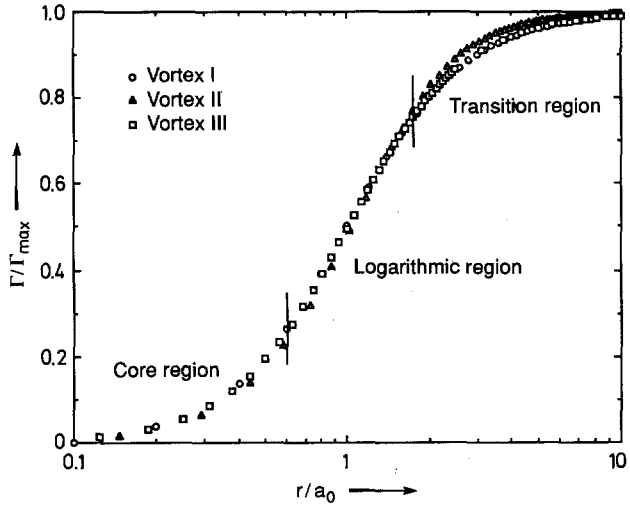

Fig. 8. Semilog plot of the normalized circulations (Γ/Γ_{max}) of three vortices with respect to the distance, r/a_0, from the center of the vortex

clear and axisymmetric, implying that this flow is quite two-dimensional. The horizontal and vertical lines in the interferograms are grid lines inscribed on the window of the test section. The measured density and pressure distributions of these vortices along with their curve-fits are shown in Fig. 5(a), (b), and (c). For the axisymmetric, compressible and viscous flow, with the assumption that the vortex center is convecting with the freestream velocity, the radial momentum equation with respect to the vortex center can be expressed as follows:

$$\frac{\partial v_r}{\partial t}+v_r\frac{\partial v_r}{\partial r}+\frac{1}{\rho}\frac{\partial P}{\partial r}-\frac{v_\phi^2}{r}-\frac{2}{\rho}\left(\frac{\partial}{\partial r}\mu\frac{\partial v_r}{\partial r}+\frac{\mu}{r}\frac{\partial v_r}{\partial r}-\frac{\mu v_r}{r^2}\right)=0 \qquad (7)$$

This equation can be simplified by considering the results of Fig. 6, which shows the evolution of the vortex with time. This pictures were taken at a 50 μs interval, which is equivalent to travelling a distance of 10 core radii. It can be noticed that the convecting vortex maintains its structure throughout the test time and remains very axisymmetric, which implies that this vortex is highly two-dimensional in spite of the side wall effects. After comparison of distributions of density and pressure at each time to estimate the temporal evolution of the vortex structure, the radial velocity into the vortex center was found to be much smaller (by at least four orders of magnitude) than the tangential velocity of the vortex [Bershader (1988)].

So, all terms involving the radial velocity v_r can be neglected in the radial momentum equation. The expression for the tangential velocity becomes,

$$v_\phi^2 = \frac{r}{\rho}\frac{\partial p}{\partial r} \tag{8}$$

The resultant tangential velocity profiles of vortices are shown in Fig. 7. By comparing these velocity profiles with the vortex model used by Sculley (1975), which is expressed as

$$v_\phi = \frac{\Gamma}{2\pi r}\left(\frac{r^2}{r^2+a_0^2}\right) \tag{9}$$

where U_∞ is the convection velocity, r is the distance from the vortex center, a_0 is the core radius, it was found that the maximum circulation, $\hat{\Gamma}(=\Gamma/U_\infty c)$, of vortex I, II, and III is 0.28, 0.37, and 0.14, respectively. The core size, a_0/c, of the vortices were found to be 0.018, 0.024, and 0.015, respectively. These core radii are much smaller than those of typical tip-trailing vortices. McAlister and Takahashi (1991) found the core radius of trailing vortex with a NACA 0015 to be 5.5% of the chord. Mason and Marchman (1973) also measured trailing vortex structure with a NACA 0012 and reported the core radius to be 6% of the chord. Figure 8 is a semilog plot for the normalized circulation distributions of the vortices with respect to r/a_0. The data of three vortices fits well into a curve for the core and the logarithmic region, but does not fit well in the transition region. The result is qualitatively very similar to the measurements of Tung et al. (1983) on the rotor-tip vortices using hot-wire anemometry (as well as other results given in Table 1) even though the present results are for a starting vortex. The proportionality constant in the linear region of the plot, is given by 0.43, and is close to the value of 0.39 by Tung et al. (1983), 0.49 by Nielsen and Schwind (1971), 0.44 reported by Corsiglia et al. (1973), 0.51 by Hoffman and Joubert (1963), 0.50 by Phillips (1981), and 0.53 by Uberoi (1979).

The curve-fit results are as follows:

1) Core region:

$$\Gamma/\Gamma_{max} = 0.80(r/a_0)^2, \qquad 0 \le r/a_0 < 0.62$$

2) Logarithmic region:

$$\Gamma/\Gamma_{max} = 0.51 + 0.43\ln(r/a_0), \qquad 0.62 \le r/a_0 \le 1.8$$

3) Transition region:

$$\Gamma/\Gamma_{max} = 1 - 0.80\exp[-0.65(r/a_0)], \qquad 1.8 < r/a_0$$

4 Conclusions

The present study indicates:

1. Highly two-dimensional, shock-induced vortices can be generated in a shock tube.
2. Independent measurement of density (by holographic interferometry) and pressure (by miniature Kulite transducers) can be used to obtain the tangential velocity and the circulation distribution of the vortex.
3. A set of empirical formulae was found for the structure of an almost two-dimensional compressible, vortex. The proportionality constants in the logarithmic region of the normalized circulation distributions were found to be 0.43 ± 0.01.
4. The circulation distribution can be normalized in a way that is independent of the angle of attack of the vortex generator and the freestream velocity.

References

Bershader, D. 1988: Foundation of the blade-vortex interaction problem: Structure and behavior of trailing compressible vortices. Summary Report to the U. S. Army Research Office, Stanford University, Stanford

Corsiglia, V. R.; Schwind, R. G.; Chigier, N. A. 1973: Rapid scanning, three- dimensional hot wire anemometer surveys of wing tip vortices. J. Aircraft 10, No. 12

Erickson, G. E. 1982: Vortex flow correlation. ICAS Paper 82-6.6.1

Hall, M. G. 1966: The structure of concentrated vortex cores. Progress in Aeronautical Sciences 7:53–110

Hariharan, P. 1985: Optical Interferometry, Academic Press, Orlando.

Hoffmann, E. R.; Joubert, P. N. 1963: Turbulent line vortices. J. Fluid Mech 16:395–411

Lee, S.; Bershader, D.; Rai, M. M.; 1991: An experimental and computational study of 2-D parallel blade-vortex interaction. AIAA Paper 91–3277, Baltimore.

Lee, S.; Bershader, D. 1992: On head-on parallel blade-vortex interaction. To be published in AIAA Journal

Lee, S. 1992: Strong parallel blade-vortex interaction and noise propagation in helicopter flight. Ph.D. Dissertation, Stanford Univ., CA

Mandella, M.; Bershader, D. 1987: Quantitative study of the compressible vortex: generation, structure and interaction with airfoil. AIAA Paper 87–0328, Reno

Mason, W. H.; Marchman III, J. F. 1973: Far-field structure of aircraft wake turbulence. J. Aircraft, 10, No. 2

McAlister, K. W.; Takahashi, R. K. 1991: NACA 0015 wing pressure and trailing vortex measurements. NASA Technical Paper 3151

McCormick, B. W.; Tangler, J. L.; Sherrieb, H. E. 1968: Structure of trailing vortices. J. Aircraft 5, No. 3:260–267

Nielsen, J. N.; Schwind, R. C. 1971: Aircraft wake turbulence and its detection, 413–454 plenum.

Phillips, W. R. C. 1981: The turbulent trailing vortex during roll-up. J. Fluid Mech. 105:451–467

Saffman, P. G. 1973: Structure of turbulent line vortices. Physics of Fluids 16 No. 8:1181–1188

Sculley, M. P. 1975: Computation of helicopter rotor wake geometry and its influence on rotor harmonic loads. ASRL TR-178-1, MIT.

Tung, C.; Pucci, S. L.; Caradonna, F. X., Morse, H. A. 1983: The structure of trailing vortices generated by model rotor blades. Vertica, 7, No. 1:33–43

Uberoi, M. S. 1979: Mechanisms of decay of laminar and turbulent vortices. J. Fluid Mech. Vol. 90 part 2:241–255.